LESSONS FROM 1-MW PROTON RCS BEAM TUNING

Hideaki Hotchi# for the J-PARC RCS beam commissioning group
J-PARC center, Japan Atomic Energy Agency, Tokai, Naka, Ibaraki, 319-1195 Japan

Abstract

Via a series of the injector linac upgrades in 2013 and 2014, the J-PARC 3-GeV RCS got all the hardware parameters required for the 1-MW design beam operation. This paper presents the recent high intensity beam experimental results in the RCS including the first 1-MW trial, mainly focusing on our approaches to beam loss issues that appeared on the process of the beam power ramp-up.

INTRODUCTION

The J-PARC 3-GeV Rapid Cycling Synchrotron (RCS) is the world's highest class of high-power pulsed proton driver aiming at the output beam power of 1 MW [1]. The injector linac delivers a 400-MeV H^- beam to the RCS injection point, where it is multi-turn charge-exchange injected through a 300-μg/cm^2-thick carbon stripping foil over a period of 0.5 ms. RCS accelerates the injected protons up to 3 GeV with a repetition rate of 25 Hz, alternately providing the 3-GeV proton beam to the Material and Life Science Experimental Facility (MLF) and to the following 50-GeV Main Ring Synchrotron (MR) by switching the beam destination pulse by pulse.

In the last summer shutdown in 2013, the ACS linac section was installed [2], by which the injection beam energy from the linac was upgraded from 181 MeV to the design value of 400 MeV. In addition, in this summer shutdown in 2014, the front-end system (IS and RFQ) of the linac was replaced [3], by which the maximum peak current of the injection beam was increased from 30 mA to the design value of 50 mA. Via these series of the injector linac upgrades, the RCS has got all the design parameters. Thus the RCS is now in the final beam commissioning phase aiming for the 1-MW design output beam power.

Fig. 1 shows the history of the RCS beam operation. Since the start-up of the user program in December, 2008, the output beam power from the RCS has been steadily increasing as per progressions in beam tuning and hardware improvements [4,5]. The output beam power for the routine user program has been increased to 300 kW as planned to date. In addition to such a routine user operation, the RCS have intermittently been continuing the high intensity beam tests toward the design output beam power of 1 MW. As shown in Fig. 1, the RCS successfully achieved high intensity beam accelerations of up to 539-573 kW for both injection energies of 181 MeV and 400 MeV before and after the installation of the ACS. Besides, the RCS has very recently conducted the first 1-MW trial right after the replacement of the front-end system. The most important issues in increasing the output beam power are control and minimization of beam loss to keep the machine activation within the permissible level. This paper presents the experimental results of these series of recent high intensity beam tests in the RCS mainly focusing on our approaches to beam loss issues that appeared on the process of the beam power ramp-up.

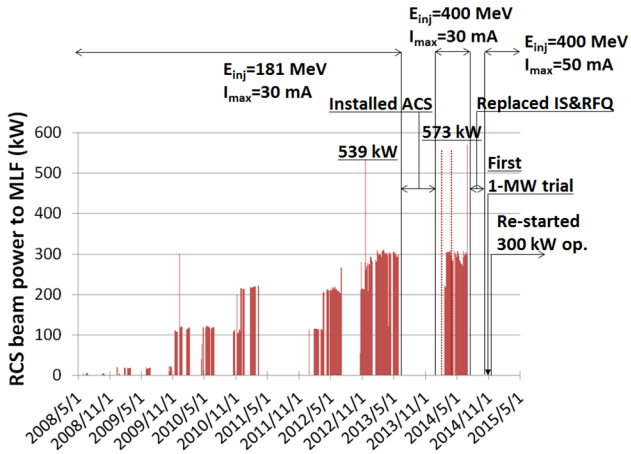

Figure 1: History of the RCS output beam power.

HIGH INTENSITY BEAM TESTS OF UP TO 553-573 kW

In April (Run#54) and June (Run#56), 2014 after installing the ACS, the RCS conducted high intensity beam tests of up to 553 (Run#54)-573 (Run#56) kW with the upgraded injection energy of 400 MeV, using a 0.5 ms-long injection pulse with a peak current of 24.6 (Run#54)-25.5 (Run#56) mA and a chopper beam-on duty factor of 60%. In these beam tests, the operating point was set at (6.45, 6.42), where the systematic beam loss measurements were performed with various injection painting parameters and beam intensities.

Painting parameter dependence of beam loss (Run#54)

In order to minimize space-charge induced beam loss at the low energy, the RCS employs injection painting both for the transverse and longitudinal phase spaces [6]. On the transverse plane, correlated painting with a painting emittance of 100π mm mrad (ε_{tp}) was applied. On the other hand, for longitudinal painting [7,8], the momentum offset injection of 0.0, –0.1 and –0.2% (Δp/p) was tested in combination with superposing a 2nd harmonic rf with an amplitude of 80% (V_2/V_1) of the fundamental rf. As an additional control in longitudinal painting, the phase sweep of the 2nd harmonic rf was also employed during injection from –100 to 0 degrees (ϕ_2) relatively to that of the fundamental rf.

#hotchi.hideaki@jaea.go.jp

ISBN 978-3-95450-173-1

Painting parameter ID

Parameter ID	ϵ_{tp} (π mm mrad)	V_2/V_1 (%)	ϕ_2 (degrees)	$\Delta p/p$ (%)
1	–	–	–	–
2	100	–	–	–
3	–	80	−100	–
4	–	80	−100	−0.1
5	–	80	−100	−0.2
6	100	80	−100	–
7	100	80	−100	−0.1
8	100	80	−100	−0.2

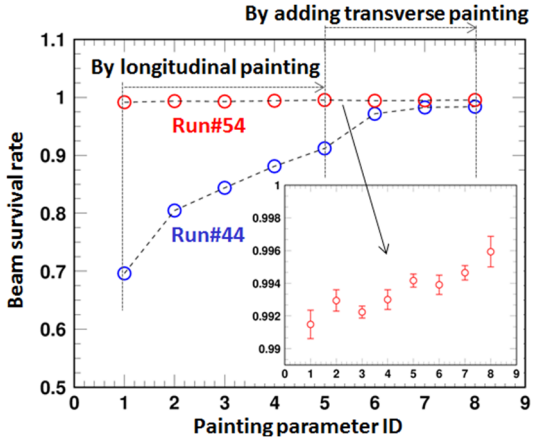

Figure 2: Beam survival rates measured with the systematic combinations of transverse and longitudinal painting (IDs 1 to 8), where the red circles correspond to the data taken for the injection energy of 400 MeV with a beam intensity of 553 kW, while the blue ones are the old data taken for the lower injection energy of 181 MeV with a similar beam intensity of 539 kW before installing the ACS linac.

Fig. 2 shows the beam survival rates measured with the systematic combinations of transverse and longitudinal painting (IDs 1 to 8), where the red circles correspond to the data taken for the injection energy of 400 MeV with a beam intensity of 553 kW (4.60×10^{13} ppp), while the blue ones are the old data (Run#44 in November, 2012) taken for the lower injection energy of 181 MeV with a similar beam intensity of 539 kW (4.49×10^{13} ppp) before installing the ACS linac.

As shown by the blue circles in Fig. 2, the larger painting parameter dependence was observed for the lower injection energy of 181 MeV, since the space-charge effect is more critical. In this case, 30%-big beam loss appeared with no painting. But this beam loss was drastically decreased from ID 1 to ID 5 by longitudinal painting, and from ID 5 to ID 8 by adding transverse painting. The plots (a) and (b) in Fig. 3 show tune footprints without and with injection painting calculated at the injection energy of 181 MeV with a beam intensity of 539 kW. As shown in the plot (a), a core part of the beam particles crosses various low-order systematic resonances for the case with no painting. Such particles on the resonances suffer from emittance dilutions. This is the main cause of the 30%-big beam loss observed with no painting. But the space-charge tune depression of (a) is well mitigated to (b) by injection painting, which results in the significant beam loss mitigation from IDs 1 to 8.

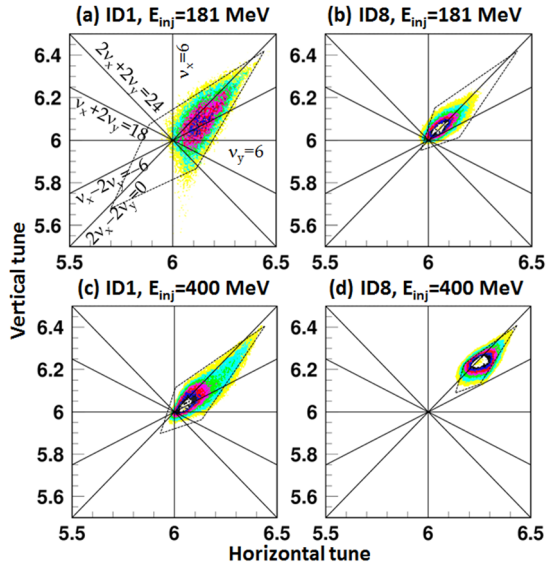

Figure 3: Tune footprints without (ID 1) and with (ID 8) injection painting calculated at the injection energy of 181 MeV with a beam intensity of 539 kW (top) and at the injection energy of 400 MeV with a beam intensity of 553 kW (bottom).

Fig. 2.

As shown by the red circles in Fig. 2, the beam survival was still improved for the higher injection energy of 400 MeV. This results from the further space-charge mitigation through the injection energy upgrade from 181 MeV to 400 MeV, as shown in the lower plots (c) and (d) of Fig. 3. The painting parameter dependence for the red circles is nearly flat, but this case also has a similar dependence to that for the blue circles, as shown in the inset of Fig. 2; the beam loss was reduced from ID1 to ID5 by longitudinal painting, and from ID5 to ID8 by adding transverse painting.

The above experimental data clearly shows the enormous gain from the injection energy upgrade this time as well as the excellent ability of injection painting.

Intensity dependence of beam loss (Run#56)

Next, the intensity dependence of beam loss was measured with the injection energy of 400 MeV, where the painting injection parameter was fixed to ID8. In this measurement, the beam intensity was varied from 107 kW (0.889×10^{13} ppp) to 573 kW (4.775×10^{13} ppp) by thinning the number of the intermediate pulses while maintaining the injection pulse length at 0.5 ms. This type of intensity variation does not change both the injection painting condition and the foil hitting rate during injection.

The top-left plot in Fig. 4 shows the beam loss monitor signals at the collimator section measured over the first 3 ms in the low energy region with various beam intensities from 107 kW to 573 kW. In this figure, one can clearly see the time structure of beam loss and its intensity dependence. The top-right plot in Fig. 4 shows the intensity dependence of beam loss amount evaluated from the integration of the beam loss monitor signal. The beam

ISBN 978-3-95450-173-1

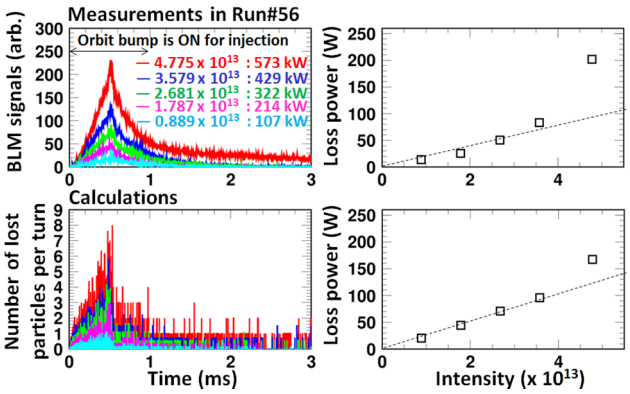

Figure 4: (Top-left) Intensity dependence of beam loss monitor signals at the collimator section measured over the first 3 ms in the low energy region with various beam intensities from 107 kW to 573 kW. (Top-right) Intensity dependence of beam loss amount estimated from the integration of the beam loss monitor signal. (Bottom) Corresponding numerical simulation results.

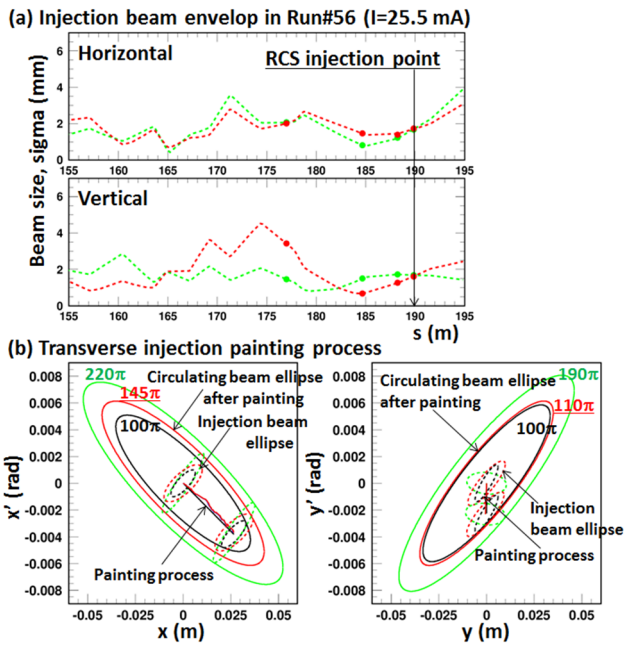

Figure 5: (a) Injection beam envelop reconstructed by the model fitting to the measured injection beam profiles (circles) before (dashed-green) and after (dashed-red) the Twiss parameter correction. (b) Transverse painting process, where the black ellipses correspond to the design one, while the other ellipses show the painting process estimated from the actual injection beam quality before (green) and after (red) its Twiss parameter correction.

loss amount shows a linear response up to the 429-kW intensity beam, but the extra beam loss increase occurs for the 573-kW intensity beam. This empirical intensity dependence of beam loss was well reproduced by the corresponding numerical simulations, as shown in the bottom plots in Fig. 4. This numerical simulation implied that the extra beam loss arises from large amplitude particles formed through the transverse injection painting

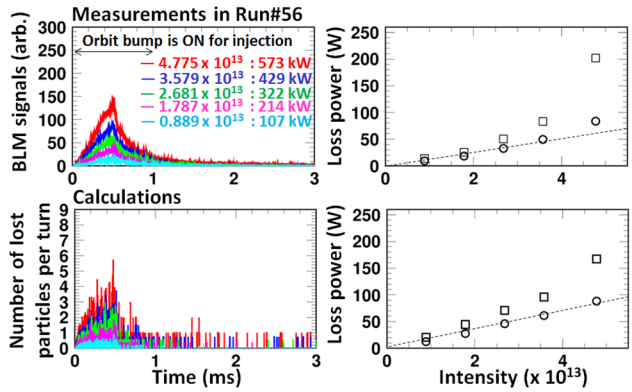

Figure 6: (Top) Similar results to the top plots in Fig. 4, observed after the Twiss parameter correction of the injection beam. (Bottom) Corresponding numerical simulation results.

process. Fig. 5-(b) shows the transverse injection painting process. The black solid ellipse in the figure shows the design painting area of 100π mm mrad, which is formed from the design beam emittance (0.25π mm mrad, rms, un-normalized) and Twiss parameter of the injection beam. But, in fact, the linac beam had a larger beam emittance than the design; 0.60π (horizontal) and 0.54π (vertical) mm mrad. In addition, its Twiss parameter at the RCS injection point had not been adjusted well at that time. Due to such a large injection beam emittance and its un-adjusted Twiss parameter, terribly large amplitude particles, which deviate from the design painting range of 100π mm mrad, are formed through the injection painting process, as shown by the green solid ellipse in Fig. 5-(b). The numerical simulation confirmed that such large amplitude particles cause the extra beam loss for the higher intensity beam in combination with the space-charge effect. Based on this analysis, we tried to mitigate the extra beam loss first by adjusting the injection beam Twiss parameter.

Further beam loss reduction by adjusting the Twiss parameter of the injection beam (Run#56)

Fig. 5-(a) shows the injection beam envelop along the injection beam transport line reconstructed by the model fitting to the measured injection beam profiles. The injection beam Twiss parameter at the RCS injection point was evaluated from this beam envelop analysis, and corrected so that the injection beam ellipse matches the circulating beam ellipse with the design painting emittance. The red solid ellipse in Fig. 5-(b) shows the painting area estimated after the correction. It is still larger than the design, since the large emittance of the injection beam remains un-touched, but it well came to fit within the permissible range. By this effort, the beam loss was well mitigated from Fig. 4 to Fig. 6 as expected. The peak value of the beam loss at the end of injection was decreased, and the following long tail beam loss was also well mitigated, with the result that the intensity dependence of beam loss

ISBN 978-3-95450-173-1

amount got to have a linear response up to the 573-kW intensity beam as shown in the top-right plot in Fig. 6. These observations were well reproduced by the corresponding numerical simulations, as shown in the bottom plots in Fig. 6. The beam loss after the injection beam adjustment appears only for the first 1 ms of the beam injection, and also its amount shows a linear response for the beam intensity. These empirical results conclude the beam loss of up to the 573-kW intensity beam is well minimized and its remaining beam loss is mainly from foil scattering during injection.

THE FIRST 1-MW TRIAL

Right after the high intensity beam tests mentioned in the last section, J-PARC had a long beam shutdown from July to September, 2014 to install the new front-end system. After completing the installation, beam tuning and tests were resumed from the linac at the end of September, 2014. Via the initial beam tuning of the linac, the RCS conducted the first 1-MW trial in October, 2014 (Run#57) at the same operating point of (6.45, 6.42) and with the same injection painting parameter of ID8. The maximum input beam intensity in this high intensity beam test reached 8.61×10^{13} ppp, using a 0.5 ms-long injection pulse with the higher peak current of 45.9 mA and a chopper beam-on duty factor of 60%, which corresponds to 1.033-MW output beam power from RCS.

Quality of the injection beam with the higher peak current of 45.9 mA (Run#57)

From the beam envelop analysis in Fig. 7-(a), the beam emittance (rms, un-normalized) for the 45.9-mA injection beam was evaluated to be 0.957π (horizontal) and 0.564π (vertical) mm mrad. Thus the 45.9-mA injection beam had a larger beam emittance than that in the previous high intensity beam test (Run#56) conducted with the peak current of 25.5 mA before replacing the front-end system. Therefore, the deviation of the painting area from the design still got worse especially on the horizontal plane as compared to that in Run#56, as shown in Fig. 7-(b), though the injection beam ellipse was similarly corrected at the injection point. Consequently, there occurs a larger imbalance between the horizontal and vertical painting areas. The present beam emittance for the 45.9-mA injection beam is 2-4 times larger than the design value of 0.25π mm mrad. As is mentioned later, this injection beam does not lead to serious issues in the RCS to date, but its quality has to be improved from now on in order to obtain the better quality for the 3-GeV beam that meets the requirements from the downstream facilities as well as to minimize beam loss in the RCS.

Result of the first 1-MW trial (Run#57)

Fig. 8 shows the circulating beam intensity measured over 20 ms from injection to extraction. As shown in the figure, the input beam intensity was gradually increased from 252 kW toward 1 MW by changing the beam thinning parameter. The beam intensity was smoothly increased up to 773 kW with no significant beam loss.

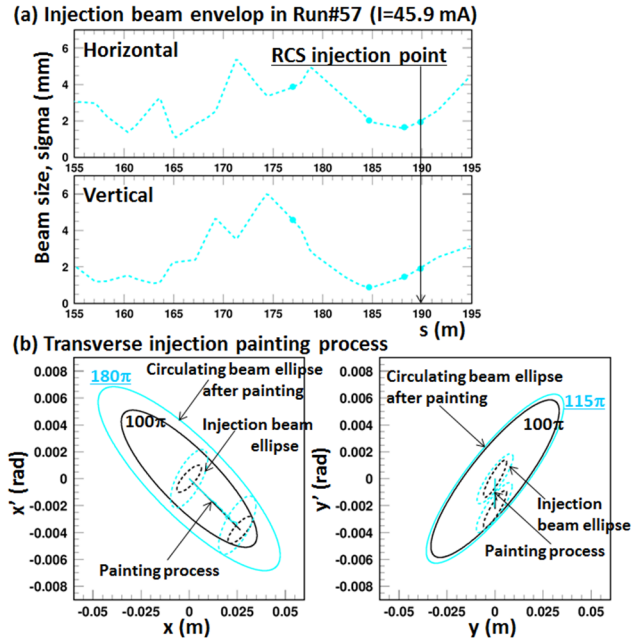

Figure 7: (a) Injection beam envelop reconstructed by the model fitting to the measured injection beam profiles (circles) after the Twiss parameter correction. (b) Transverse painting process, where the black ellipses correspond to the design one, while the light-blue ones are the painting process estimated from the actual injection beam quality after its Twiss parameter correction.

But, when the beam intensity got to over 800 kW, the anode power supply of the RF cavity system suddenly stumbled due to the over current. The circles in Fig. 9 show the anode current measured as a function of the beam intensity [9]. In the RCS, the multi-harmonic feed-forward method (h=2, 4 and 6) is employed for beam loading compensation [10]. Therefore the required anode current increases following the ramp-up of the beam intensity. The blue line in the figure corresponds to the present interlock level for the anode current. Thus, in the present condition, the required anode current surpasses the interlock level when the beam intensity gets to over 800 kW. This is the main cause of the RF trip this time.

We are now considering several possible measures against this issue. The first one is to use a remaining margin of the anode power supply. The interlock level is now set to 110 A, but it can be safely increased up to 115 A in design. The second one is to shift the resonant frequency of the RF cavity by removing a capacitor. The resonant frequency shift of the RF cavity acts to tilt the beam intensity dependence of the anode current from the circles to the squares in Fig. 9, by which the required anode current for the 1-MW beam acceleration decreases from 124 A to 109 A [9]. By taking these possible measures, the anode current required for the 1-MW beam acceleration comes to stay within the limit. After taking these quick measures, we will re-try the 1-MW beam acceleration in

ISBN 978-3-95450-173-1

December, 2014. We are also planning to increase the anode power supply itself to secure sufficient

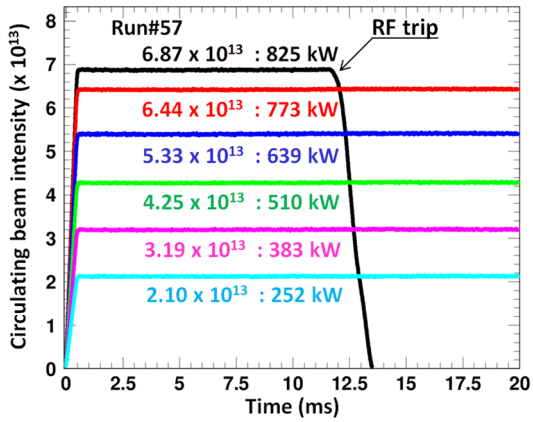

Figure 8: Circulating beam intensity measured over 20 ms from injection to extraction.

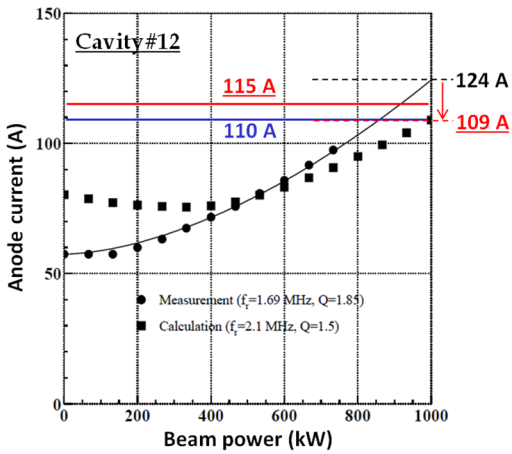

Figure 9: Anode current for the RF cavity#12 measured as a function of the beam intensity (circles). The intensity dependence of the anode current can be tilted to the squares by the resonant frequency shift of the RF cavity.

margin for the 1-MW beam acceleration using the next summer shutdown period in 2015, aiming to start up the 1-MW routine user operation in October, 2015 as originally planned.

Though the 1-MW beam acceleration was not reached this time, the RCS successfully demonstrated high intensity beam accelerations of up to 773 kW. The upper plot in Fig. 10 shows the beam loss monitor signals at the collimator section measured over the first 3 ms in the low energy region with various beam intensities from 252 kW to 773 kW. As shown in the plot, the beam losses mainly appear for the first 1 ms of the beam injection. In addition, their time structures are very similar to each other, and also to the beam loss data taken in the previous high intensity beam test (Run#56) given in Fig. 6. Inevitably, the beam loss amount nearly shows a linear response for the beam intensity, as shown in the lower plot in Fig. 10. These empirical results similarly conclude the beam loss of up to the 773-kW intensity beam is nearly minimized and its remaining beam loss is mainly from foil scattering during injection. The beam loss for the 773-kW intensity beam was estimated to be less than 0.2%, most of which

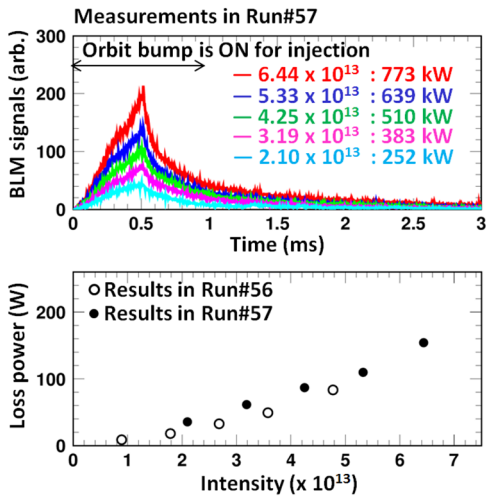

Figure 10: (Top) Intensity dependence of beam loss monitor signals at the collimator section measured over the first 3 ms in the low energy region with various beam intensities from 252 kW to 773 kW. (Bottom) Intensity dependence of beam loss amount estimated from the integration of the beam loss monitor signal in the top plot (closed circles), where the open circles correspond to the previous data shown in the top-right plot of Fig. 6.

was well localized at the collimator section. The beam loss power of 160 W is still much less than the 4-kW collimator capability.

SUMMARY

Via a series of the injector linac upgrades in 2013 and 2014, the RCS conducted the first 1-MW trial in October, 2014. Although the 1-MW beam acceleration was not reached this time due to the RF trip, the RCS successfully demonstrated a high intense beam acceleration of 773 kW at a low-level intensity loss of less than 0.2%. Most of the 0.2%-beam loss, which is mainly from foil scattering during injection, was well localized at the collimator section. The beam loss power of 160 W is still much less than the 4-kW collimator capability.

We plan to re-try the 1-MW beam acceleration in December, 2014 after taking several quick measures against the RF trip. The RCS beam commissioning is steadily progressing, and now we are nearly approaching the final goal.

REFERENCES

[1] JAERI-Tech 2003-044 and KEK Report No. 2002-13.
[2] H. Ao et al., PRST-AB **15**, 011001 (2012).
[3] H. Oguri, Proc. of IPAC2013, WEYB101.
[4] H. Hotchi et al., PRST-AB **12**, 040402 (2009).
[5] H. Hotchi et al., PTEP **2012**, 02B003 (2012).
[6] H. Hotchi et al., PRST-AB **15**, 040402 (2012).

ISBN 978-3-95450-173-1

[7] F. Tamura et al., PRST-AB **12**, 041001 (2009).
[8] M. Yamamoto et al., NIM, A **621**, 15 (2010).
[9] M. Yamamoto, Private communication.
[10] F. Tamura et al., PRST-AB **14**, 051004 (2011).

ISBN 978-3-95450-173-1